CRIMSON Project: Full-scale Turbine Demonstration By Tank Tests

Massimo Falchi, Patrick Cronin, Clement Courade, Conor Dillon, Francesca Magionesi, Mohammad Rafiei, and Francesco Salvatore

***Abstract*—The results of demonstration tests of a full-scale hydrokinetic turbine for river and tidal sites, are presented at the conclusion of the EU-funded CRIMSON project. The turbine features a 3-bladed crossflow, 9.0 m^2 capture area rotor, representing one module of the ORPC RivGen© technology. A comprehensive matrix of operational trials was performed to characterize the turbine hydrodynamic performance and the efficiency of the power conversion system. An advanced blade structural monitoring equipment based on fiber-optics strain sensors was implemented and validated. The full-scale turbine tests were carried out at the hydrodynamics testing infrastructure at the Institute of Marine Engineering of the Italian National Research Council (CNR-INM). This facility, among the largest of its kind globally, provided fully controlled and repeatable conditions that allowed to deliver a high-quality dataset on system performance and realiability, contributing to develop new knowledge for the enhancement of hydrokinetic turbine technology.**

***Index Terms*—Hydrokinetic energy, river and tidal current, cross-flow turbines, full-scale demonstration, tank testing.**

I. Introduction

THE production of green energy from streaming waters represents an appealing solution among innovative renewable sources to reduce the dependency from fossil fuels in the short term [1]. Instream hydrokinetic turbine technology has reached commercial readiness level, with MW-scale plants in operation and in the pipeline for the next few years [2]. In parallel with the exploitation of tidal sites offshore, inland rivers also provide relevant conditions for instream turbines. The operational environment in a river with flow confinement limitations is adequate for compact kW-scale devices. Nonetheless, continuous production delivers large amounts of energy, with significant contributions to the decarbonization of remote communities. Moreover, riverine projects contribute to develop fundamental knowledge for the design of hydrokinetic turbines for offshore installations.

The CRIMSON project (www.crimsonproject.eu) was a consortium of five partners from Ireland, Italy and Germany, with a 3 Millions Euro budget co-funded by the European Union under the Horizon Europe Programme. The 39 months action concluded in May 2024 was aimed at the development and demonstration of innovative solutions to increase the efficiency and reduce the LCoE of hydrokinetic turbines. The cross-flow turbine technology taken as a reference in the project was the RivGen© Power System developed by the ORPC company, and operational at sites in North and South America (www.orpc.co).

The enhancement of system reliability and sustainability was the main focus in the project. The utilization of carbon fiber recycled from large wind turbine blades was investigated, the composite blade manufacturing process was improved, and the design of new rotor components was delivered. A distinguishing feature of the CRIMSON project is that the improved design was demonstrated through structural tests and operational trails at full scale, with a 5 m wide, 1.8 m diameter rotor. Details of structural tests conducted at University of Galway can be found in [3].

In this paper, the results of operational trails of the full-scale CRIMSON turbine are presented. The activity was carried out at the hydrodynamics testing towing tank infrastructure at the Institute of Marine Engineering of the National Research Council (CNR-INM), Rome, Italy (www.inm.cnr.it). Demonstration tests provided a comprehensive characterization of the turbine hydrodynamic performance, and the efficiency of the power conversion system. An advanced fiber-optics strain sensors technology for foil structural monitoring was also implemented and validated.

The technical challenge of testing a full-scale, fully equipped turbine in a towing tank infrastructure was the subject of a detailed design of experiment work documented in [4].

II. The Full Scale Turbine and the Testing Infrastructure

A. The RivGen© Power System by ORPC

The cross-flow turbine developed in the CRIMSON project reflects the layout of the RivGen© Power Sys-

Part of a special issue for ICOE 2024. Manuscript submitted 28 March 2025; Accepted 10 April 2025. Published 15 August 2025.

This article has been subject to a single-blind peer review by a minimum of two reviewers.

This work was partially supported by the EU-H2020 CRIMSON project, Grant no. 971209.

Massimo Falchi (e-mail: massimo.falchi@cnr.it), Francesca Magionesi (e-mail: francesca.magionesi@cnr.it), Mohammad Rafiei (email: mohammad.rafiei@cnr.it) and Francesco Salvatore (e-mail: francesco.salvatore@cnr.it) are with the Institute of Marine Engineering of the Italian National Research Council (CNR), Via di Vallerano, 139, I-00128 Rome, Italy.

Patrick Cronin (e-mail: pcronin@orpc.co), Clement Courade (e-mail: ccourade@orpc.co), and Conor Dillon (e-mail: cdillon@orpc.co) are with ORPC Ireland Ltd, Dublin, Ireland.

Digital Object Identifier:
https://doi.org/10.36688/imej.8.299-308

tem designed by ORPC to generate emission-free electricity from river currents (top Fig. 1). The device operates fully submerged with no visible features and key components are manufactured in advanced composite materials that are optimized for performance and lifecycle. A single RivGen© unit combines two helically twisted crossflow rotors, with a rated power output of 40 kW at 2.25 m/s and 80 kW at 3.5 m/s.

In the CRIMSON project, a full-scale single rotor of the RivGen© Power System was the subject of demonstration tests. The 5.0 m wide rotor with diameter $D = 1.8$ m, equipped with generator and gearbox is here referred to as the CRIMSON turbine. Bottom Fig. 1 shows the turbine ready for testing during the CRIMSON project.

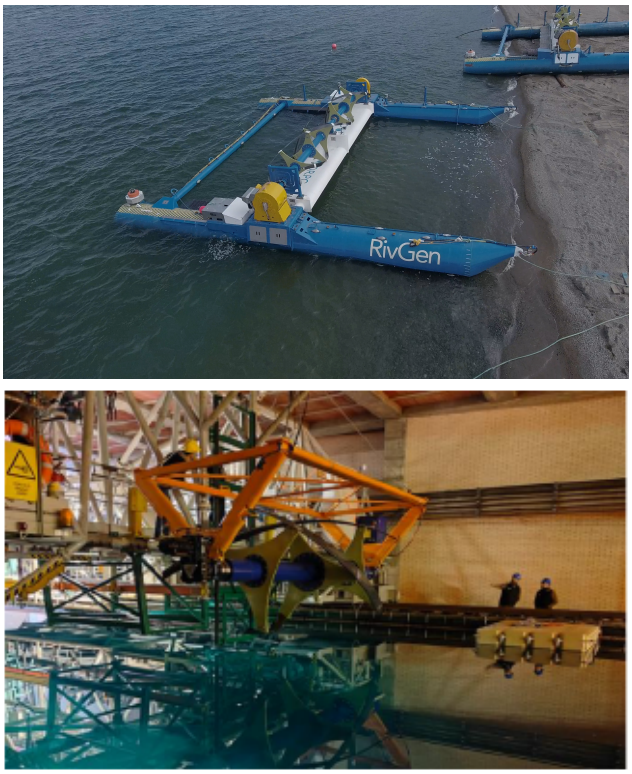

Fig. 1. The RivGen© Power System by ORPC. Top: river installation (Igiugig, Alaska, USA). Bottom: the CRIMSON turbine ready for deployment at CNR-INM (Rome, Italy).

B. The Calm Water Towing Tank at CNR-INM

The calm water towing tank at the Institute of Marine Engineering of the National Research Council (CNR-INM, Rome, Italy), is among a few hydrodynamics testing facilities in Europe and globally where a full-scale device with the characteristics of the CRIMSON turbine can be operated under fully controlled and repeatable conditions. The tank is 460 m long, 13.5 m wide and 6.5 m deep, and is equipped with a towing carriage powered by 4x92 kW electric motors. The carriage speed can reach 15 m/s and is controlled with a 0.1% precision. In the towing tank environment, the operating conditions of an instream hydrokinetic device are reproduced by towing the device at imposed speed against water at rest in the tank [5], [6]. Figure 2 shows the tank (top) and the towing carriage (bottom).

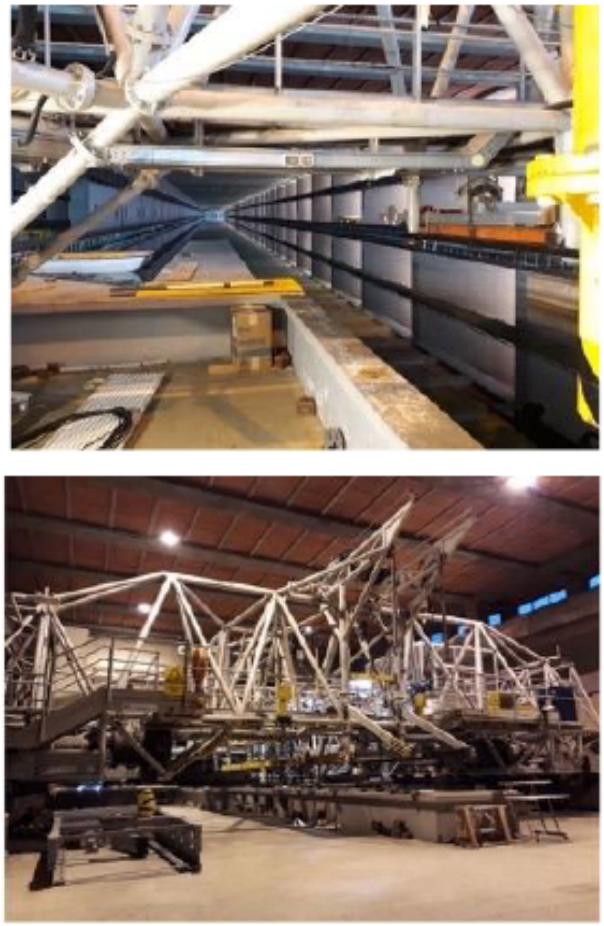

Fig. 2. The calm water towing tank facility at CNR-INM. View of the tank (top) and of the towing carriage (bottom).

A sketch of the tank cross section with the turbine in the operating condition is depicted in Fig. 3. The turbine immersion at rotor shaft was set equal to one rotor diameter. Recalling the rotor is 5.0 m wide and the diameter is 1.8 m, its frontal area is about 10% of the tank cross section area, which determines acceptable flow confinement effect conditions.

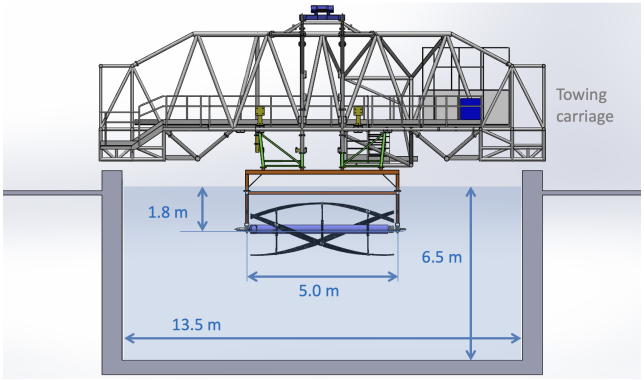

Fig. 3. Sketch of the turbine in the tank and main dimension (front view).

III. Turbine Power Management, Measuring Sensors and Data Acquisition

A. Turbine power and control management

The CRIMSON turbine was equipped with a 15kW Permanent Magnet Synchronous Generator (PMSG) by Bauer Gear Motor. The generator was a shaft mounted submersible model, fitted with a mechanical parking brake and a gearbox with transmission ratio 46.16:1.

The generator was connected to a Yaskawa GA700 Variable Frequency Drive (VFD) housed in a custom-built electrical cabinet, powered by tri-phase 400 V from the carriage electrical system. The cabinet also housed braking choppers and a Honeywell Remote Terminal Unit (RTU) to operate the VFD as a master-slave pair. To interface with the RTU, and control the system during testing, the RTU was connected by a suitable communication protocol (Modbus TCP) with a panel-mounted computer (PC). The panel provided operator's access by an Ignition© human-machine interface (HMI) system. In addition to device control, the interface featured charts and plots for live monitoring, save and export of turbine speed and electrical power data streams. Figure 4 shows the generator set and the components housed inside the cabinet. The PC with human-machine interface was mounted on the cabinet door (not shown).

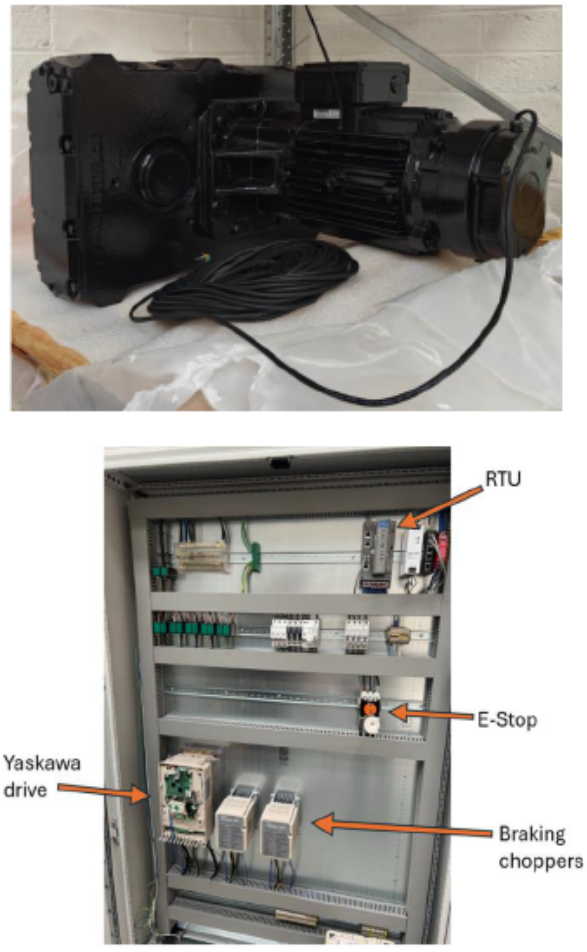

Fig. 4. The generator set (top) and the electrical cabinet (bottom).

B. Sensor equipment

The PC installed on the electrical cabinet was also dedicated to the acquisition of data from sensors to characterize the structural response of the rotor blades as strain levels. This type of measurement represents a distinguishing aspect in the CRIMSON testing program, with advanced Fiber Bragg Grating (FBG) optical sensors installed on the surface of one of the rotor foils. An XGTR interrogator by PhotonFirst© interprets the signals and sends them to the PC on the electrical cabinet, where the data can be visualized and recorded through the XGOS software developed by PhotonFirst©. The foil was equipped with 34 FBG sensors distributed on 5 custom-made fiber optics. Sensors locations on the instrumented foil are shown in Fig. 5.

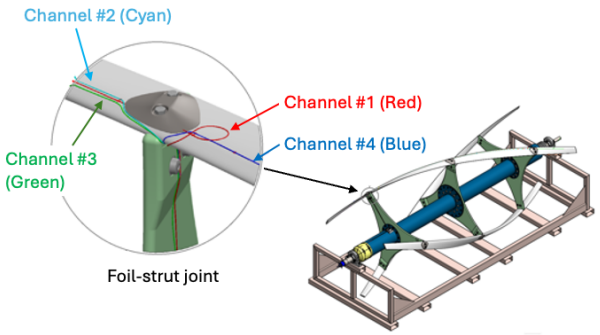

Fig. 5. Location of fiber-optics sensors on the rotor blade.

Other sensors were installed to characterize the device hydrodynamic performance, the flow field perturbation around the turbine, and the structural excitation induced on the turbine supporting frames.

The turbine mechanical torque was measured by a load pin mounted on the turbine frame. The sensor measured the force F_p on the frame structure to resist the action of the rotor. An indirect measurement of the mechanical torque was then obtained as $Q_m = d_p F_p$, where d_p is the distance between the pin position and the rotor axis. The turbine rotational speed n measured by a shaft encoder allowed to determine the mechanical power as $P_m = 2\pi n Q_m$ (n in rps).

The mechanical loads transmitted by the turbine to the carriage were measured by tri-axial Piezo-electric force-link sensors by PCB Piezotronics Inc., with high-frequency response, and maximum capacity of 49 kN (normal force) and 18 kN (in-plane components). The load cells were bolted at the four flanges coupling the turbine frame and the supporting frame fixed to the carriage. In addition to that, three mono-axial accelerometers were mounted on the turbine frame to characterize the vibratory excitation on the supporting structures. Acceleration transducers model ASW-5A by Kyowa Electronic Instruments Co. were used, with rated capacity of $\mp$ 49.03 m/s^2 and frequency response of 100 Hz. Figure 6 illustrates the position of sensors installed on the turbine and on the supporting frames.

Other sensors not shown in Fig. 6 were installed around the turbine to characterize the perturbed flow

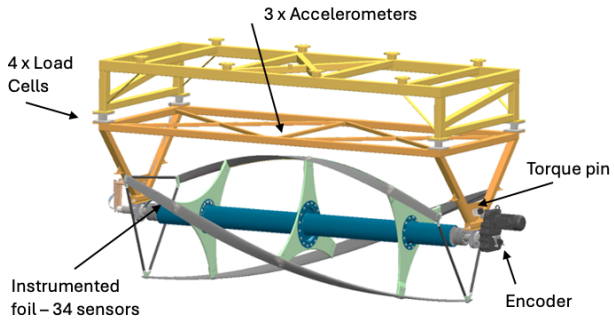

Fig. 6. Position of sensors on the turbine and supporting frames.

around the turbine. The velocity field was observed by two Hydronics TH-D Pitot-tube, single-component sensors for the measurement of the relative flow speed in the towing direction. The PT_{up} sensor was placed at distance $2D$ upstream of the turbine, in the mid longitudinal plane. The PT_{ps} sensor was placed at distance $2.25D$ at portside of the rotor, and colinear with the rotor shaft. Both sensors were place at same immersion of the rotor shaft.

The free-surface perturbation was measured by two AECO SUC-P150-UIH ultrasound wave probes with 1400 mm range. These sensors were installed in the mid longitudinal plane, upstream (WP_{up}) and downstream (WP_{do}) at a distance of $0.65D$ from the rotor shaft.

C. Data acquisition

The output signals from the load pin, the Pitot-tube velocimeters, the ultra-sound wave probes, the load cells and the accelerometers were processed by the Data Acquisition (DAQ) system routinely used at CNR-INM facilities. The system also processed the actual carriage towing speed, to be compared with the nominal value imposed by the carriage driver. The DAQ is based on DEWE43-A boards by DEWESoft. Each board provides 16 input channels, equally divided into analog and digital types. Simultaneous sampling rate up to 200kS/sec is supported. Four boards were used during tests. The hardware was controlled by the DEWESoftX 2023 software operated from a workstation onboard the carriage for data processing, visualization and storage.

The CNR-INM facility DAQ system was combined with the corresponding system in the panel-mounted PC of the ORPC electrical cabinet described above, where turbine electrical power, rotational speed, and data streams from the FBG optical sensors were acquired. The synchronization between the two DAQs was obtained via a common trigger signal. Sensor data was acquired with a frequency rate of 1 Hz for the turbine electrical power and rotational speed, 1 kHz for the FBG foil strain, and 5 kHz for all the other data.

IV. Test Matrix, Set-up and Test Procedure

A full range of turbine operating conditions from cut-in flow speed to rated flow speed was considered. Towing speed V was varied from 1.0 to 2.25 m/s with 0.25 m/s steps. For each condition, a variable turbine rotational speed n was set to obtain a full sweep of the Tip Speed Ratio (TSR or λ)

$$\lambda = \frac{\pi n D}{V}. \tag{1}$$

A total of 242 runs covering the full tank length were carried out over more than 30 testing days.

Top Fig. 7 provides a graphical representation of the test matrix, with all the (TSR, RPM) conditions parametrized with respect to the towing speed V, whereas RPM = 60 n is the rotational speed in round per minute. The combination of V and RPM values was chosen to realize, for each towing speed case, a TSR sweep between 1.6 and 3.8, with few exceptions for the highest V and TSR cases.

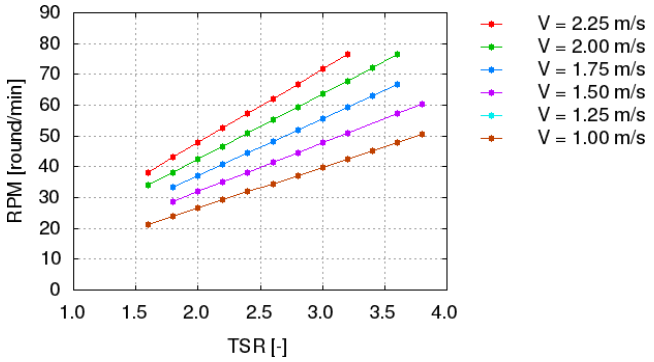

Fig. 7. Test matrix: towing speed V, turbine TSR and rotational speed RPM.

The Reynolds number Re referred to the total velocity V_{tot} incoming to turbine foils and blade chord lenght $C_0 = 0.2$ m, measured at mid span follows as

$$Re = \frac{C_0 V_{tot}}{\nu} = \frac{C_0 \sqrt{V^2 + (2\pi n R)^2}}{\nu} \tag{2}$$

where ν is the fresh water kinematic viscosity at temperature of 13.7 ^{o}C from averaged data across the testing period. Using the expression in Eq. (2), the Reynolds number varied between 0.37E6 to 0.88E6 at $V = 1$ m/s, and 0.65E6 to 1.29E6 at $V = 2.25$ m/s.

For each towing run, a single (V, TSR) condition was tested. Figure 8 shows a representative time-series of the relative flow velocity measured by the Pitot-tube upstream of the turbine, with indication of carriage start and stop instants. According to the towing speed, the acquisition time with stable conditions varied approximately between 120 and 280 seconds.

The turbine operational trials in the tank were carried out according to standard procedures for hydrokinetic turbines (IEC TS 62600-200, [7]) and recommended procedures from the International Towing Tank Conference (ITTC 7.5-02-07-03.9, [8]).

The following turbine operation procedure was applied. The drive is operated in speed control, by setting a shaft rotational speed. Before carriage start, the VFD in the electrical cabinet supplies energy to rotate the turbine at the imposed RPM. Once the carriage starts moving, the flow speed induces a torque on the turbine, and the generator transitions from motoring to generating power. The generated power is dissipated

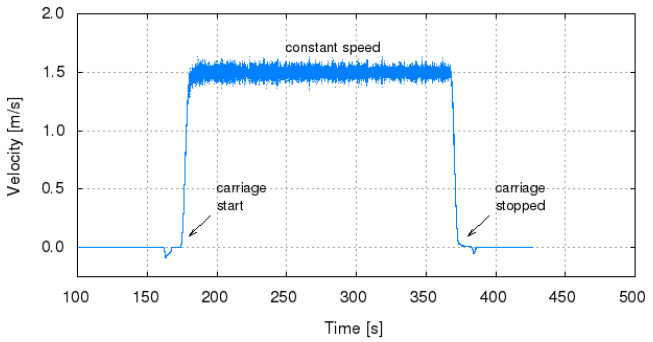

Fig. 8. Incoming flow speed from carriage start to stop during a run.

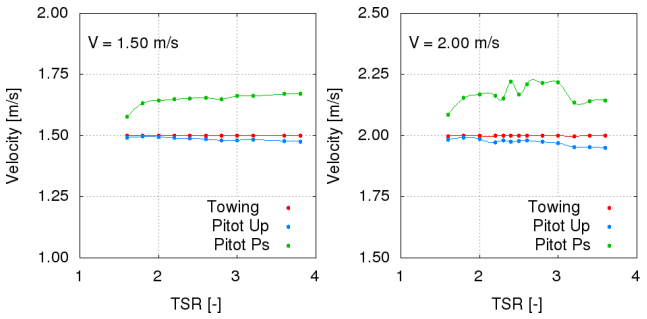

Fig. 9. Flow velocity upstream of the turbine (Up) and at portside (Ps). Towing at $V = 1.5$ m/s (left) and $V = 2.0$ m/s (right).

by two braking resistors with braking choppers connected to the VFD.

V. Experimental Results

A TeraByte scale dataset was collected from towing tank trials. The measured data streams were processed using standard approaches for time series with high-frequency sampling. Raw data detrending was applied and outliers were removed from the datasets. The samples were collected in bins and statistical analysis was performed. Data processing software included Matlab© and in-house built scripts in Python and Fortran90. Processed data are presented as mean values (dotted lines) and vertical bars proportional to the standard deviation of sample data. For a generic data set f_i with N samples, the standard deviation (STD, or σ) is defined as

$$\sigma(f) = \sqrt{\frac{1}{N}\sum_{i=1}^{N}\left(f_i - \hat{f}\right)^2} \tag{3}$$

where $\hat{f}$ is the mean value of the N samples.

A. Flow conditions

The flow field perturbation induced by the turbine during operation at different towing speed and TSR was investigated by the Pitot-tube velocimeters and ultra-sound wave probes described in Section III-B.

Figure 9 presents the flow velocity measured by the Pitot tube upstream of the turbine (Up) and at portside (Ps), for two representative towing speeds $V = 1.5$ and 2.0 m/s, over a full TSR sweep. Sensor data are compared with the actual carriage speed which, as expected, is extremely constant for all conditions. The results show that at $2D$ upstream of the turbine, the flow is slightly decelerated, with increasing effect as TSR increases, whereas a 10-12% flow acceleration is observed in the channel between the turbine and the tank side wall.

Wave elevation measurements are described in Fig. 10, where the results for three representative towing speed cases are plotted versus TSR. Positive elevation values denote wave crests, that is, free surface above the level under calm water conditions. Results show a limited water surge in front of the turbine, associated with flow deceleration and pressure rise, see Fig. 9. This corresponds to a more intense lowering of the free surface level just downstream of the device. The increase in measured data STD with towing speed can be explained with the additional perturbation induced by the wet portions of the turbine frames.

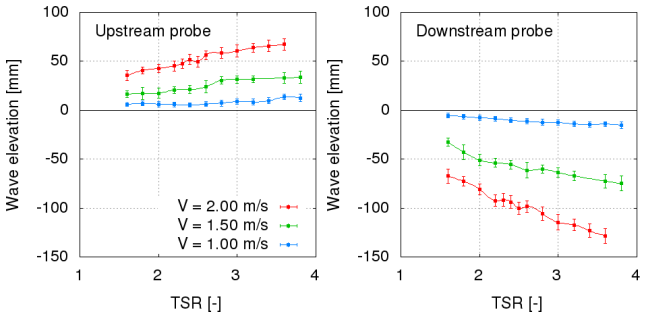

Fig. 10. Wave elevation upstream (left) and downstream (right) of the turbine, $V = 1.0$, 1.5, 2.0 m/s.

B. Turbine performance

The results of turbine hydrodynamic performance were obtained from the mechanical torque Q_m measured by the load pin sensor described in Section III-B. Recalling the mechanical power can be written as $P_m = 2\pi n Q_m$ (n in rps), the corresponding torque and mechanical power coefficients are

$$C_{Q_m} = \frac{Q_m}{\frac{1}{2}\rho A R V^2}, \tag{4}$$

$$C_{P_m} = \frac{P_m}{\frac{1}{2}\rho A V^3} = \lambda C_{Q_m}, \tag{5}$$

where $\rho = 998$ Kg/m3 is fresh water density, $A = 9$ m^2 is the frontal area of the turbine rotor, and $R = D/2$.

Figure 11 shows the mechanical torque over a TSR range for all towing speed conditions from 1.0 to 2.25 m/s. Mean values and STD are presented in normalized form, dividing all values by the peak value $Q_{m,ref}$ at the highest towing speed. For some velocity and TSR conditions, fluctuations of mean value curves are observed. From the analysis of raw data and towing run repeats, the fluctuations can be explained with a relatively low precision of the force pin sensor used to determine the torque.

The standard deviation of mechanical torque data is presented in Fig. 12 as percent of the mean value. With few exceptions, the most part of acquisitions have STD between 10 and 20% of the mean torque. The amount of

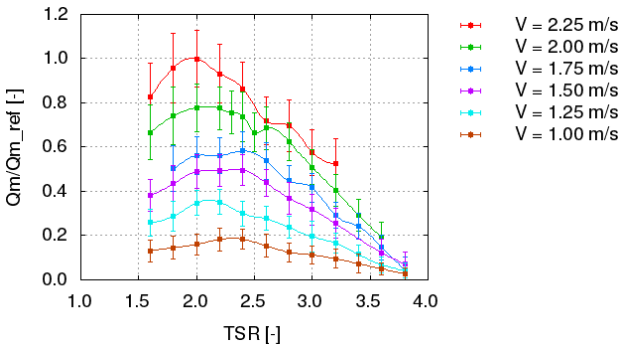

Fig. 11. Normalized mechanical torque (mean value and STD).

data scattering seems not directly related to flow speed, whereas a trend with larger STD as TSR increases is observed.

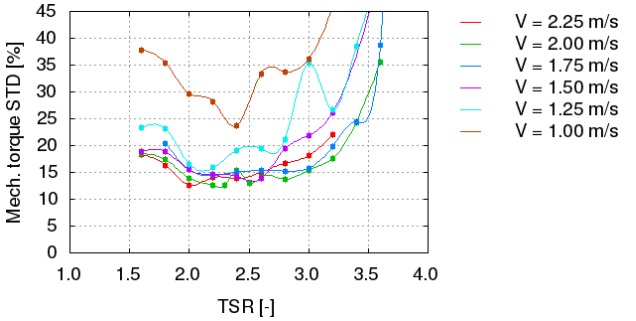

Fig. 12. Mechanical torque, STD as percent of mean value.

The mechanical power P_m and the corresponding power coefficient C_{P_m} are presented in Fig. 13. Mean values and STD are normalized with respect to the peak power value at the highest towing speed. The effect of the above mentioned fluctuations in measured torque are apparent. At low flow speed, the peak power condition is approximately at TSR = 2.5, and shifts to lower TSR values at higher flow speed. Comparing in bottom Fig. 13 the mean values of the power coefficient at given TSR value, a regular trend with respect to the flow speed cannot be found.

The electrical power delivered by the generator was determined as $P_e = VI$, with tension V (Volts) and current I (Ampere) output from the generator. Quantities P_e and its coefficient C_{P_e} (adapted from Eq. 4) are presented in Fig. 14 as mean values normalized with respect to the corresponding peak values at the highest towing speed. Different to the mechanical power discussed above, measurements at constant flow speed and variable TSR present regular distributions, with very limited oscillations in correspondence to the peak power conditions that occur between TSR values 2.2 and 2.6, with the peak condition at lower TSR as the flow speed increases. For a given TSR, the power coefficient increases with flow speed, as effect of the increasing Reynolds number, Eq. (2). In particular, C_{P_e} curves at $V = 1.5$ m/s and higher, present small variations with flow speed.

It can be concluded that at the highest flow speed conditions in the present test matrix, Reynolds independence of measured turbine power is achieved. The

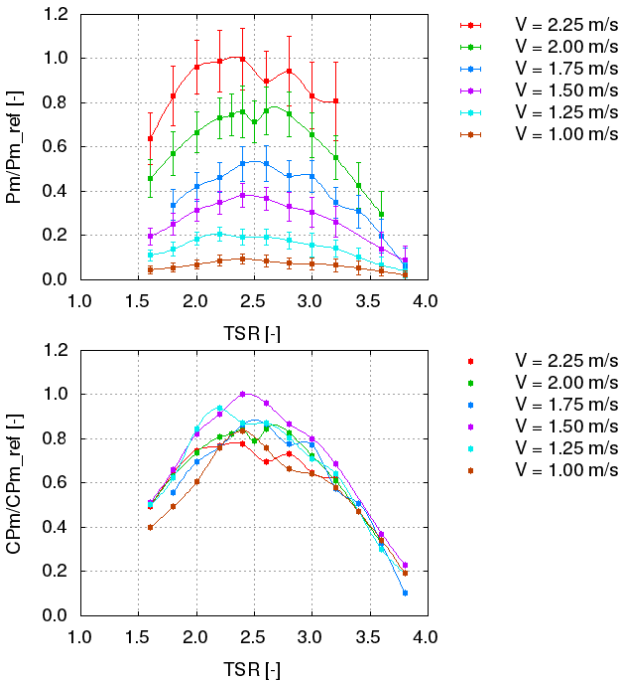

Fig. 13. Mechanical power (mean value and STD, top) and power coefficient (mean value, bottom).

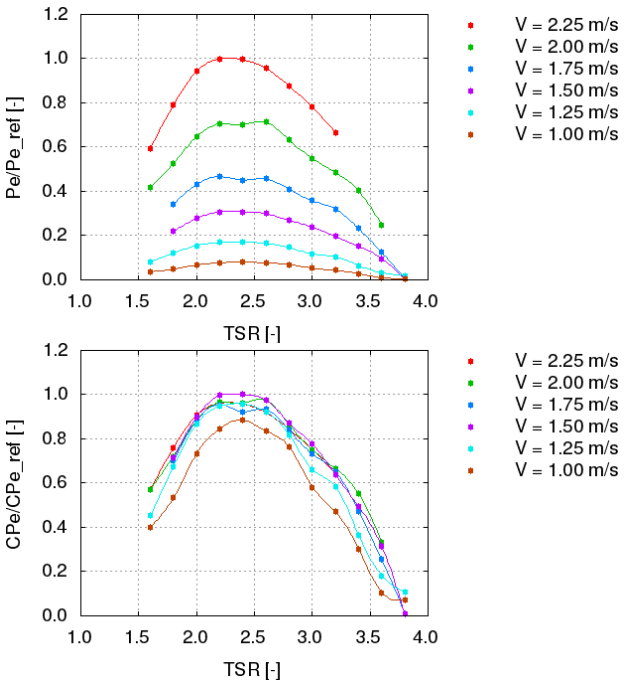

Fig. 14. Electrical power (mean value, top) and power coefficient (mean value, bottom).

power coefficient determined in this condition can be taken to extrapolate turbine performance at higher flow speed.

The results of output power measurements were also used to identify the peak power condition as a function of flow speed and turbine rotational speed. By plotting the normalized electrical power $P_e/P_{e,ref}$ as a function of rotational speed in RPM, the curves parametrized with towing speed V in Fig. 15 are obtained. The black line denotes a third-order polynomial connecting the estimated peak power points for each flow speed (Maximum Power Point Tracking, MPPT). From mea-

sured data, the following polynomial expression was determined

$$P_{MPPT} = P_{e,ref} \left(\frac{RPM}{54.05} \right)^3 \quad (6)$$

This semi-empirical analytical definition of the MPPT condition can be used in power control strategies to maximize the performance of turbines operating in highly fluctuating flow speed regimes.

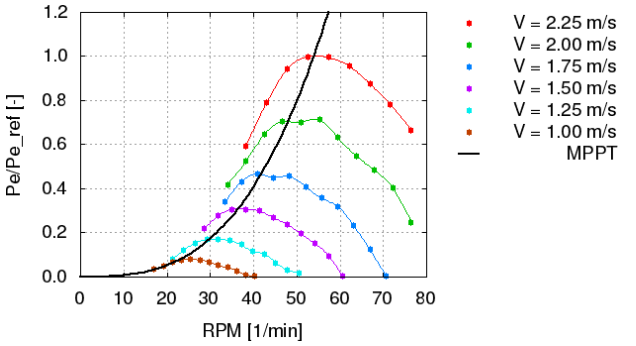

Fig. 15. Normalized electrical power as function of rotational speed RPM. Estimated MPPT condition by polynomial law in Eq. (6).

The comparison of measured mechanical and electrical power allows to estimate the efficiency of power conversion in the drivetrain specifically realized for turbine demonstration trials in the CRIMSON project. The conversion efficiency calculated from mean values as $\eta = (P_m - P_e)/P_m$ is plotted in Fig. 16. The observed fluctuations in the mechanical power data determine a significant scatter of quantity η across the TSR range at all speeds (left Fig. 16). However, a general trend with a larger efficiency as the flow speed increases can be observed. From right Fig. 16, one obtains an averaged conversion efficiency $\eta = 0.75$ at $V = 1.25$ m/s and a higher value of approximately $\eta = 0.9$, for the $V = 2.25$ m/s condition.

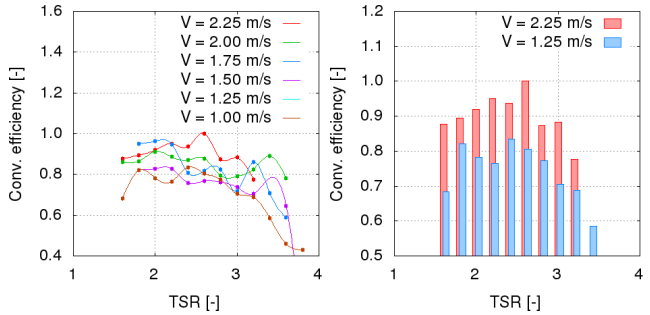

Fig. 16. Power conversion efficiency: flow velocity from 1.0 to 2.25 m/s (left), and high, low flow speed cases compared (right).

C. Foil structural monitoring

The FBG optical sensors described in Section III-B allowed to capture the maximum strain around each joint where blades are connected to the rotor struts (Fig. 5) and to characterize the strain distribution along the span of the foil. Figure 17 shows strain levels on the instrumented foil during operation at $V = 2$ m/s and TSR = 2.4. The chart shows the strain evolution over two rotations at each strut (with 2 sensors on both sides of the struts). The blue lines correspond to the starboard strut, the orange lines denote the middle strut, and the green lines are for the strut at portside.

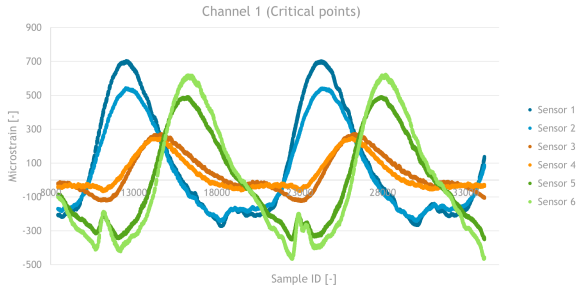

Fig. 17. Time series of strain at blade/strut joints. Towing speed $V = 2$ m/s and TSR = 2.4.

For a representative sensor (channel 1), Fig. 18 clearly shows a linear relationship between microstrain and rotational speed (TSR) for the same flow speed. An exponential relationship is also noticeable between strain and flow speed at constant TSR.

These trends highlight that the structural response of the foil can be predicted for a given flow condition.

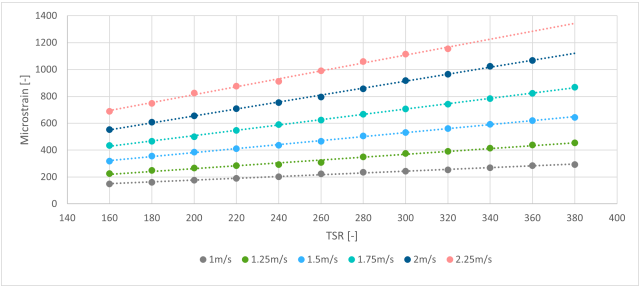

Fig. 18. Evolution of strain versus TSR/rotational speed at constant towing speed values from 1 to 2.25 m/s.

D. Turbine loadings

The utilization of the tri-axial load cells described in Section III-B was aimed at the characterization of the hydrodynamic loads generated by the rotor during operation. The four coupling flanges at the top of the turbine frame (Fig. 6) were identified as the most convenient locations to install the sensors. The positions were below the free surface level and adequate water resistance protection was ensured by sensor characteristics and installation procedure.

Unfortunately, the analysis of data streams from all the 12 channels (3-force components for each load cell) revealed random oscillations, and non-physical decaying or constant-value signals. From the inspection done by the staff at the testing facility and support by the sensor manufacturer, unexpected water intrusion was found to explain the spurious readings obtained. For this reason, the results of load cell data streams is not considered in the present analysis.

E. Vibratory excitation to supporting frames and carriage

One of the objectives of towing tests was the identification of the structural characteristics of the turbine assembly. The measurements were also used to compare with the results of numerical simulations carried out during the design of experiment phase, as discussed in [4]. For this analysis, the three accelerometers described in Section III-B were installed on the frame supporting the turbine. The mono-axial sensors were mounted to measure vibrations in the turbine axial direction (Acc. no. 1), in the flow direction (Acc. no. 2), and in the vertical direction (Acc. no. 3). The position of the accelerometers is shown in Fig. 19 with representative results of data analysis described here below. This set-up allowed to determine the modal parameters (natural frequencies) of the turbine frame and the level of structural vibrations transmitted from the rotor blades to the carriage through the supporting frames.

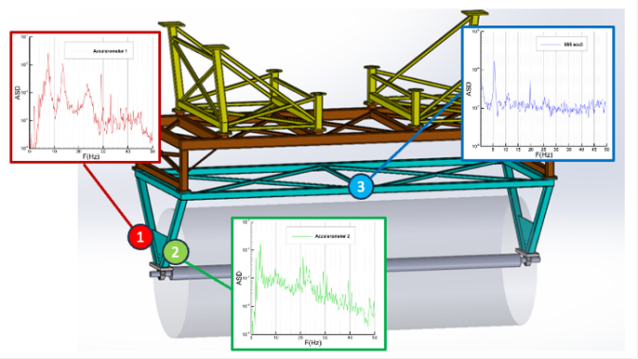

Fig. 19. Position of the accelerometers on the turbine frame and representative excitation results (Auto Spectral Density, Eq. (7)).

Examples of accelerometer measurements are given in Fig. 20, where data streams from the accelerometer no. 1 at TSR = 2.4 and different combinations of towing speed and rotational speed, are depicted over a time interval of 0.2 seconds (1000 samples). As expected, the vibration levels increase significantly with the carriage speed and the intensity of the hydrodynamic loads.

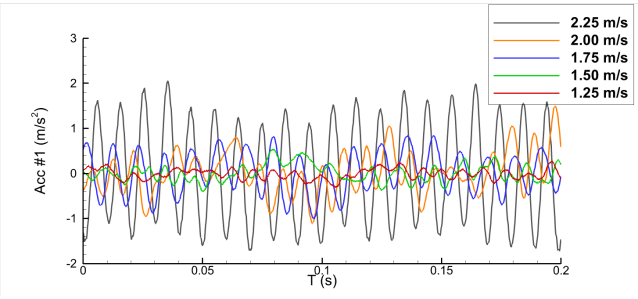

Fig. 20. Time series of accelerometer no. 1 data. Turbine operation at TSR = 2.4 and variable towing speed.

Raw data from the accelerometers were processed using Matlab© scripts. A convenient representation of signals in the frequency domain was obtained by evaluating the Auto Spectral Density (ASD) of measured time series.

For a continuous time signal $x(t)$, the ASD $S_{xx}(f)$ is obtained as the Fourier transform of the autocorrelation function $R_{xx}(t) = E[x(t)x(t+\tau)]$, where the operator $E[\ ]$ denotes the expected value. The ASD follows as (see, *e.g.*, [9])

$$S_{xx}(f) = \int_{-\infty}^{\infty} R_{xx}(\tau) e^{-j2\pi f \tau} d\tau. \tag{7}$$

This data analysis allowed to identify general features of the structural response. For all tested conditions, the frequency spectra of the accelerometer signals present distinctive peaks associated with the natural frequencies of the structure. The signals exhibit a broad frequency range due to the structural damping, as highlighted in Fig. 21 for a representative case at the highest flow speed. Superimposed on these peaks, the accelerometer ASDs also reveal peaks related with the Blade Passing Frequencies (BPFs), characterized by a very narrow frequency band.

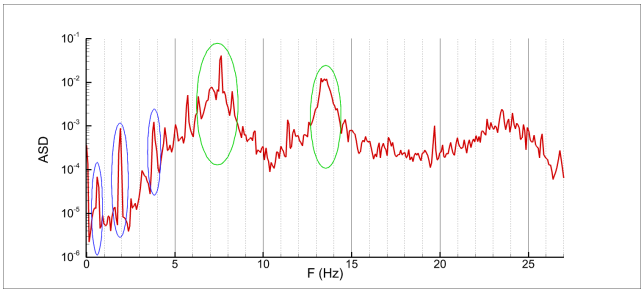

Fig. 21. ASD of accelerometer no. 1 data at TSR = 1.6 and $V = 2.25$ m/s. BPF peaks (blue) and natural frequencies peaks (green).

The plots in Fig. 22 compare the ASD by processing raw data from the three accelerometers for selected TSR and towing speed conditions. Sensors no. 1 to 3 are ordered from top to bottom.

The averaged ASD of accelerometer signals acquired at $V = 2$ m/s for different TSR is depicted in Fig. 23. The spectra exhibit three broad peaks at approximately 7, 13.5 and 23 Hz, and a narrow peak at 1.2 Hz, which could be related with the natural frequencies of the entire carriage. Moreover, in the frequency range 3.4 to 3.9 Hz (close-up area), the mean ASD of the three accelerometers shows peaks that are not exactly coincident. Further data processing by cross-correlation between signals from the same accelerometer and different turbine loading conditions (by varying RPM), allowed to better identify peaks denoting the natural response of the structure (natural frequencies). The results of this modal analysis are summarized in Table I, where the frequency of main structural peaks at the three accelerometers are presented. Recalling mono-axial accelerometers were used, their sensitivity to structure eigenmodes and frequencies largely depended on the mounting position and sensor directivity. Empty fields in Table I denote cases where the identification of a natural frequency from data streams was uncertain.

VI. Conclusions

The results of operational trials of a full-scale cross-flow hydrokinetic turbine in the EU-H2020 CRIMSON

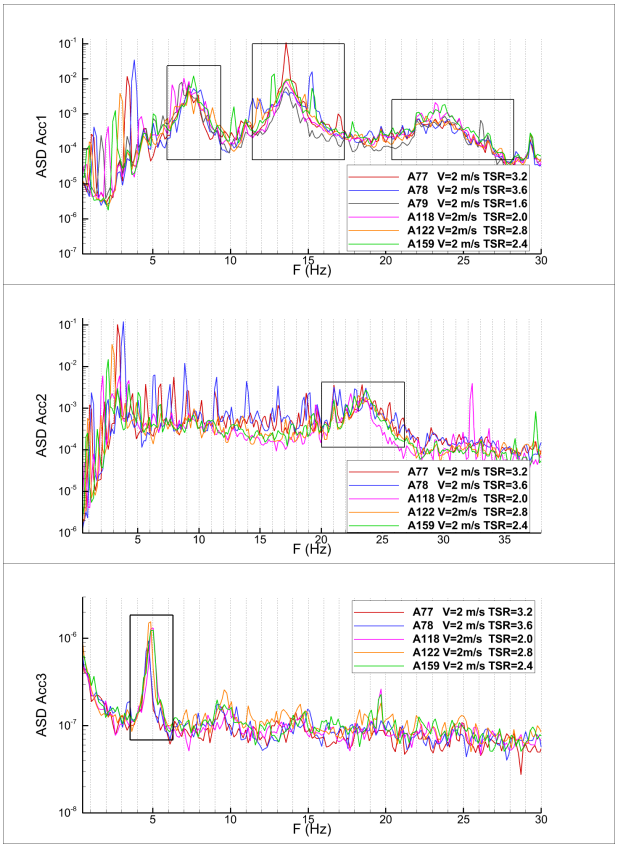

Fig. 22. ASD of accelerometer data for selected TSR and V cases. Sensors no. 1 to 3 are ordered from top to bottom.

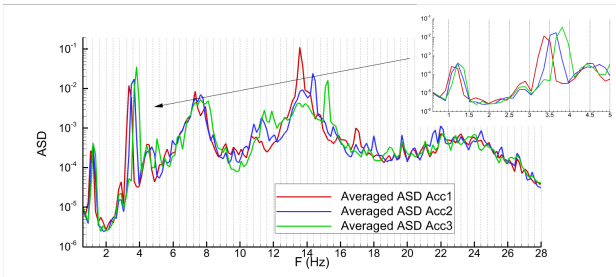

Fig. 23. Mean ASD spectra at $V = 2$ m/s by averaging data at different TSR.

TABLE I
FREQUENCY OF MAIN STRUCTURAL EXCITATION PEAKS AT ACCELEROMETERS IN FIG. 19.

Mode No.	Acc. #1	Acc. #2	Acc. #3
1	–	3.3	4.6
2	7.3	–	–
3	13.7	–	–
4	23.0	23.0	–

project have been presented. The technology addressed was representative of the RivGen© Power System by ORPC. A comprehensive characterization of device performance and structural response was carried out in the controlled and repeatable environment of the large calm water tank at CNR-INM. A detailed design of experiment study was conducted to ensure safe operations of the CRIMSON turbine across a full TSR range with flow speed from 1.0 to 2.25 m/s. The turbine was equipped with sensors to characterize the hydrodynamic performance (mechanical torque and power) and the efficiency of electrical power generation. The foil structural response was analysed by advanced FBG optical sensors to measure strain levels at key positions along the blade. The loadings and vibrations transmitted from the turbine to the supporting frames and to the towing carriage were measured by load cells and accelerometers. The flow perturbation induced by the turbine was characterized by Pitot velocimeters and ultra-sound wave probes.

Main findings from the completed test program can be summarized as follows:

- considering the size and power of the full-scale device, the operation of the CRIMSON turbine in the towing tank represented a first-of-its-kind activity. The adoption of an integrated digital design of experiment approach ensured safe and efficient operations during all phases of the test campaign.
- A comprehensive dataset of device performance and power output was generated, covering a full range of operating conditions in terms of flow speed and turbine rotational speed.
- The results of the testing program provided significant knowledge on device health-monitoring. The controlled and repeatable conditions offered by the towing tank provided an ideal environment to validate a complex fiber-optic technology for foil strain characterization.

Part of the experimental dataset is published on the SEANOE open repository [10], in accordance with the FAIR (Findable, Accessible, Interoperable, Reusable) guiding principles for research project results.

A general conclusion is that testing at large scale in large towing tanks represents an effective approach to validate design iterations at medium TRL, and de-risk the deployment of devices in the real operating environment in a river or at sea.

ACKNOWLEDGEMENT

The authors wish to thank the staff at CNR-INM calm water towing tank and laboratories for their excellent support.

REFERENCES

[1] "An eu strategy to harness the potential of offshore renewable energy for a climate neutral future - com 2020-741," September 2020. [Online]. Available: www.eur-lex.europa.eu

[2] "Tidal current energy developments and highlights," Ocean Energy Systems (OES), Tech. Rep., 2023. [Online]. Available: www.ocean-energy-systems.org

[3] V. Fakhari, T. R. Munaweera Thanthirige, M. Flanagan, C. Kennedy, Y. Jiang, M. O'Conghaile, T. Flanagan, C. Courade, P. Cronin, C. Dillon, J. Goggins, and W. Finnegan, "Theoretical and experimental transverse vibration analysis of a non-uniform composite helical tidal turbine foil," *Ocean Engineering*, vol. 309, p. 118384, 2024.

[4] M. Rafiei, F. Magionesi, F. Salvatore, M. Falchi, P. Cronin, C. Dillon, and C. Courade, "Crimson project: De-risking tank testing of large-scale hydrokinetic turbines," in *Proceedings of the International Conference on Ocean Energy (ICOE)*, 2024.

[5] A. Day, A. Babarit, A. Fontaine, Y.-P. He, M. Kraskowski, M. Murai, I. Penesis, F. Salvatore, and H.-K. Shin, "Hydrodynamic modelling of marine renewable energy devices: A state of the art review," *Ocean Engineering*, vol. 108, pp. 46–69, 2015.

[6] B. Gaurier, G. Germain, J. Facq, C. Johnstone, A. Grant, A. Day, E. Nixon, F. Di Felice, and M. Costanzo, "Tidal energy 'round robin' tests comparisons between towing tank and circulating tank results," *Int. Journal of Marine Energy*, vol. 12, pp. 87–109, 2015.

[7] "Marine energy - wave, tidal and other water current converters - part 200: Electricity producing tidal energy converters - power performance assessment," Int. Electro-technical Commission (IEC), Tech. Rep. IEC TS 62600-100, 2023.

[8] "Model tests for current turbines - recommended guideline," Int. Towing tank Conference (ITTC), Tech. Rep. 7.5-02-07-03.9, 2014. [Online]. Available: https://ittc.info/media/8372/index.pdf

[9] J. S. Bendat and A. G. Piersol, *Random Data, Anaysis and Measurement Procedures*. John Wiley and Sons, 2010.

[10] P. Cronin, C. Courade, C. Dillon, H. Knoblauch, L. Loic, M. Falchi, and F. Salvatore, "Advanced photonics for marine hydrokinetic structural health," 2024, sea Open Scientific Data Publication (SEANOE). [Online]. Available: https://doi.org/10.17882/101260